J Physiol 598.19 (2020) pp 4339–4355

The Journal of Physiology

Pathophysiological changes in inner hair cell ribbon synapses in the ageing mammalian cochlea

Jing-Yi Jeng[1,2], Federico Ceriani[1,2], Jennifer Olt[1], Steve D. M. Brown[3], Matthew C. Holley[1], Michael R. Bowl[3], Stuart L. Johnson[1,2] and Walter Marcotti[1,2]

[1]*Department of Biomedical Science, University of Sheffield, Sheffield, S10 2TN, UK*
[2]*Neuroscience Institute, University of Sheffield, Sheffield, S10 2TN, UK*
[3]*Mammalian Genetics Unit, MRC Harwell Institute, Oxfordshire, UK*

Edited by: Ian Forsythe & Michael Evans

Key points

- Age-related hearing loss (ARHL) is associated with the loss of inner hair cell (IHC) ribbon synapses, lower hearing sensitivity and decreased ability to understand speech, especially in a noisy environment.
- Little is known about the age-related physiological and morphological changes that occur at ribbon synapses.
- We show that the differing degrees of ARHL in four selected mouse stains is correlated with the loss of ribbon synapses, being most severe for the strains C57BL/6NTac and C57BL/6J, less so for C57BL/6NTac^{Cdh23+}-Repaired and lowest for C3H/HeJ.
- Despite the loss of ribbon synapses with age, the volume of the remaining ribbons increased and the size and kinetics of Ca^{2+}-dependent exocytosis in IHCs was unaffected, indicating the presence of a previously unknown degree of functional compensation at ribbon synapses.
- Although the age-related morphological changes at IHC ribbon synapses contribute to the different progression of ARHL, without the observed functional compensation hearing loss could be greater.

Abstract Mammalian cochlear inner hair cells (IHCs) are specialized sensory receptors able to provide dynamic coding of sound signals. This ability is largely conferred by their ribbon synapses, which tether a large number of vesicles at the IHC's presynaptic active zones, allowing high rates of sustained synaptic transmission onto the afferent fibres. How the physiological and morphological properties of ribbon synapses change with age remains largely unknown. Here, we have investigated the biophysical and morphological properties of IHC ribbon synapses in the ageing cochlea (9–12 kHz region) of four mouse strains commonly used in hearing research: early-onset progressive hearing loss (C57BL/6J and C57BL/6NTac) and 'good hearing' strains (C57BL/6NTac^{Cdh23+} and C3H/HeJ). We found that with age, both modiolar and pillar sides of the IHC exhibited a loss of ribbons, but there was an increased volume of those that remained.

Jing-Yi Jeng received her MSc degree in Biotechnology at National Tsing Hua University (Taiwan) and her PhD in Biomedical Science at The University of Sheffield (UK). Her research aims to understand the physiological mechanisms crucial for the development and ageing of the cochlear hair cells in the mammalian cochlea. She is a Postdoctoral Research Associate within the Hearing Research Group (https://www.sheffield.ac.uk/hearing) in the Department of Biomedical Science at The University of Sheffield (UK).

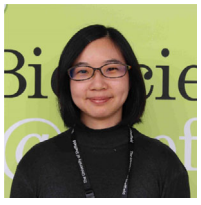

DOI: 10.1113/JP280018

These morphological changes, which only occurred after 6 months of age, were correlated with the level of hearing loss in the different mouse strains, being most severe for C57BL/6NTac and C57BL/6J, less so for C57BL/6NTac^{Cdh23+} and absent for C3H/HeJ strains. Despite the age-related reduction in ribbon number in three of the four strains, the size and kinetics of Ca^{2+}-dependent exocytosis, as well as the replenishment of synaptic vesicles, in IHCs was not affected. The degree of vesicle release at the fewer, but larger, individual remaining ribbon synapses colocalized with the post-synaptic afferent terminals is likely to increase, indicating the presence of a previously unknown degree of functional compensation in the ageing mouse cochlea.

(Received 24 April 2020; accepted after revision 24 July 2020; first published online 25 July 2020)
Corresponding author Walter Marcotti: Alfred Denny Building, Western Bank, Sheffield S10 2TN, UK.
Email: w.marcotti@sheffield.ac.uk

Introduction

Age-related hearing loss (ARHL) is the most common form of sensory deficit in the human population (Bowl & Dawson, 2019), causing a progressive, bilateral sensorineural loss associated with decreased hearing sensitivity, decreased ability to understand speech and impaired sound localization (Gates & Mills, 2005; Gordon-Salant, 2005). Damage to the hair cells has been considered the key contributor to the development of ARHL based on *in vivo* auditory measurements (Johnsson, 1974; Schuknecht & Gacek, 1993). However, recent evidence has shown that the degeneration of the type I spiral ganglion neurons (SGNs) innervating the inner hair cells (IHCs) is likely to precede hair cell degeneration in the ageing cochlea in mice and humans (Stamataki *et al.* 2006; Sergeyenko *et al.* 2013; Kujawa & Liberman, 2015; Wu *et al.* 2019). Loss of synaptic connections between the IHCs and their type I SGN afferent terminals impacts on the normal encoding of the temporal properties of sound, especially in a noisy environment (Costalupes *et al.* 1984).

In the adult mammalian cochlea, sound-induced displacement of the stereociliary bundles leads to the depolarization of IHCs and activation of the $Ca_V1.3$ Ca^{2+} channels (Platzer *et al.* 2000; Brandt *et al.* 2003; Jeng *et al.* 2020*a*), which are clustered at the cell's presynaptic active zones composed of synaptic ribbons (e.g. Frank *et al.* 2010; Zampini *et al.* 2013). Ribbons enable tethering of a large number of vesicles, allowing them to facilitate high rates of sustained synaptic transmission onto the auditory afferent fibres (e.g. Glowatzki & Fuchs, 2002; Keen & Hudspeth, 2006; Goutman & Glowatzki, 2007). At mature IHC ribbon synapses, $Ca_V1.3$ Ca^{2+} channels are coupled to glutamate-filled vesicles in either a Ca^{2+} nanodomain or a Ca^{2+} microdomain (Wong *et al.* 2014; Johnson *et al.* 2017, 2019). Each postsynaptic type I SGN forms only one synapse with an adult IHC (Pujol *et al.* 1998), with up to ∼20 afferent neurons contacting a single IHC in mice (Meyer *et al.* 2009). These SGNs are segregated around the basolateral membrane of IHCs. In the cat, while high-spontaneous-rate (low-threshold) spiral ganglion fibres preferentially contact the pillar side of IHCs (towards the outer hair cells) with small synaptic ribbons, low-spontaneous-rate (high-threshold) fibres primarily contact the modiolar side (towards the cochlear nerve) with larger synaptic ribbons (Liberman, 1978; Liberman *et al.* 1990). The physiological and morphological diversity of SGNs is likely to be important to support the wide dynamic range of sound intensity encoded by the IHCs (Winter *et al.* 1990). Currently, very little is known about how ribbon synapses in mouse IHCs, and their associated afferent connections, change with cochlear ageing, and which of those changes directly influences the temporal acquisition of ARHL.

We have identified the initial physiological and morphological changes that occur in ageing IHC ribbon synapses using mice with differing progressions of hearing loss: early-onset progressive hearing loss mice (C57BL/6J and C57BL/6NTac) and late-onset hearing loss mice (C3H/HeJ and C57BL/6NTac^{Cdh23+}). Like CBA/CaJ, C3H/HeJ mice show a very slow decline in their hearing thresholds with age (Ohlemiller *et al.* 2016). We found that with age, the ribbon synapses underwent a significant reduction in number and volume, which were correlated with the level of hearing loss in the 9–12 kHz cochlear region of the different mouse strains. C3H mice, which have relatively normal hearing at 18 months of age, had very little or no changes at their IHC ribbon synapses. Despite the synaptic morphological changes in most mouse strains, the size of the Ca^{2+} current and vesicle exocytosis was not affected with age, highlighting some degree of functional compensation at IHC ribbon synapses in the ageing cochlea.

Materials and methods

Ethics statement and animal strains

All animal work was performed at the University of Sheffield (UK), was licensed by the Home Office under the Animals (Scientific Procedures) Act 1986

(PPL_PCC8E5E93) and was approved by the University of Sheffield Ethical Review Committee (180626_Mar).

For *in vitro* experiments, male mice were killed by cervical dislocation. For *in vivo* auditory brainstem responses (ABRs) mice were anaesthetized using ketamine (100 mg kg^{-1} body weight, Fort Dodge Animal Health, Fort Dodge, IA, USA) and xylazine (10 mg kg^{-1}, Rompun 2%, Bayer HealthCare LLC, New York, NY, USA), which were administered with I.P. injection as previously described (Ingham *et al.* 2011). At the end of the procedure, mice were either killed according to schedule 1 (cervical dislocation) or recovered from anaesthesia with I.P. injection of atipamezole (1 mg kg^{-1}). Mice under recovery from anaesthesia were returned to their cage, placed on a thermal mat and monitored over the following 2–4 h. Once mice were able to move well and respond to external stimuli, the cages were returned to their holding racks.

Tissue preparation

In vitro recordings were performed from apical-coil IHCs positioned at a frequency range of ∼9–12 kHz of the mouse cochlea (Müller *et al.* 2005; see also Ceriani *et al.* 2019). Acutely dissected organs of Corti from both male and female mice were obtained from 1- and 18-month-old wild-type mice (C57BL/6N, C57BL/6J and C3H/HeJ), and the genome-edited C57BL/6NTac^{Cdh23+} mice (Mianné *et al.* 2016). The dissection procedure of the aged mouse cochlea was performed as previously described (Jeng *et al.* 2020*b*). The excised cochleae were dissected in extracellular solution composed of (in mM): 135 NaCl, 5.8 KCl, 1.3 $CaCl_2$, 0.9 $MgCl_2$, 0.7 NaH_2PO_4, 5.6 D-glucose, 10 Hepes-NaOH. Sodium pyruvate (2 mM), amino acids and vitamins were added from concentrates (Thermo Fisher Scientific, UK). The pH was adjusted to 7.48 (∼308 mmol kg^{-1}). The dissected organ of Corti was then transferred to a microscope chamber, immobilized using a nylon mesh fixed to a stainless steel ring and viewed using an upright microscope (Olympus BX51, Tokyo, Japan; Leica, DMLFS, Wetzlar, Germany; Nikon FN-1, Tokyo, Japan). The microscope chamber was continuously perfused with extracellular solution by a peristaltic pump (Cole-Palmer, Chicago, IL, USA). Hair cells were observed with Nomarski differential interference contrast (DIC) optics (63× or 60× water immersion objectives) and 15× eyepieces.

Single-cell electrophysiology

Real-time changes in membrane capacitance (ΔC_m) were recorded at near body temperature (34–37°C) and using 1.3 mM extracellular Ca^{2+} as previously described (Johnson *et al.* 2008, 2013, 2017). Recordings were obtained with an Optopatch amplifier (Cairn Research Ltd, Faversham, UK). Data acquisition was controlled by pClamp software using Digidata 1440A or 1550 boards (Molecular Devices, Sunnyvale, CA, USA). The patch pipette intracellular solution contained (in mM): 106 caesium glutamate, 20 CsCl, 3 $MgCl_2$,1 EGTA-CsOH, 5 Na_2ATP, 0.3 Na_2GTP, 5 Hepes-CsOH, 10 Na_2-phosphocreatine, pH 7.3 (294 mmol kg^{-1}). The experimental protocol consisted of a 4 kHz sine wave of 13 mV RMS, which was applied to IHCs from the holding potential of −81 mV, and was interrupted for the duration of the voltage step. The capacitance signal from the Optopatch was filtered at 250 Hz and sampled at 5 kHz. ΔC_m was measured by averaging the C_m trace over a 200 ms period following the voltage step and subtracting the pre-pulse baseline. Membrane potentials were corrected for the voltage drop across the series resistance and a liquid junction potential of –11 mV. ΔC_m experiments were performed during the local perfusion of an extracellular solution containing 30 mM TEA and 15 mM 4-AP (Fluka) to block the BK current ($I_{K,f}$) (Marcotti *et al.* 2004) and delayed rectifier K^+ currents (I_K, previously called $I_{K,neo}$ in the case of pre-hearing IHCs and $I_{K,s}$ in mature IHCs), and linopirdine (80 μM: Tocris, Bristol, UK) to block $I_{K,n}$ (Marcotti *et al.* 2003). When the concentration of blockers was ≥1 mM, NaCl was adjusted in the extracellular solution to keep the osmolality constant. The number of vesicles in the readily releasable pool (RRP) was estimated using a conversion factor of 37 aF per vesicle (Lenzi *et al.* 1999).

Auditory brainstem responses

ABRs were recorded from male and female mice between 1 and 18 months of age from the four strains listed above. Recordings were performed in a soundproof chamber (MAC-3 Acoustic Chamber, IAC Acoustic, Chandler's Ford, UK) as previously described (Ingham *et al.* 2011). Briefly, stimuli were delivered to the ear by calibrated loudspeakers (MF1-S, Multi Field Speaker, Tucker-Davis Technologies, Alachua, FL, USA) placed 10 cm from the animal's pinna. Sound pressure was calibrated with a low-noise microphone probe system (ER10B+, Etymotic, Elk Grove Village, IL, USA). Experiments were performed using customized software (Ingham *et al.* 2011) driving an RZ6 auditory processor (Tucker-Davis Technologies). Response thresholds were estimated from the resulting ABR waveform and defined as the lowest sound level where any recognizable feature of the waveform was visible. Responses were measured for clicks and stimulus pure tones of frequencies at 6, 12, 18, 24, 30, 36 and 42 kHz. Stimulus sound pressure levels were typically 0–95 dB SPL, presented in steps of 5 dB SPL. The brainstem response signal was averaged over 256 repetitions. Tone bursts were

5 ms in duration with a 1 ms on/off ramp time, which was presented at a rate of 42.6 s^{-1}.

Wave 1 amplitude and latency were measured from ABR recordings obtained by presenting mice with a pure tone (12 kHz, 75 dB SPL). We selected 12 kHz because it is close to the frequency range used for the *in vitro* work, and 75 dB SPL was the minimal value that allowed the comparison among the different mouse strains (all mice used for this analysis had hearing thresholds below 75 dB at 12 kHz). An initial automatic identification of Wave 1 was carried out using a custom software routine based on the *find_peaks* function of the scipy.signal Python module (Python 3.7, Python Software Foundation, Wilmington, DE, USA) (Virtanen *et al.* 2019). Results were manually reviewed and, if required, adjusted to the correct peak. The Wave 1 amplitude was calculated as the difference between the amplitude of the first peak and the first trough of the ABR waveform; the latency was calculated as the delay of the Wave 1 peak from the beginning of the recording. Since the distance of the speaker from the animal is 10 cm (see above), this leads to a delay in the signal of ∼0.3 ms, which was not corrected for.

Immunofluorescence microscopy

Dissected inner ears from the above mouse strains were fixed with 4% paraformaldehyde in PBS (pH 7.4) for 20 minutes at room temperature. Cochleae were dissected, rinsed three times for 10 min in PBS, and incubated for 1 h at room temperature in PBS supplemented with 5% normal goat or horse serum and 0.5% Triton X-100. The samples were then incubated overnight at 37°C with the primary antibody in PBS supplemented with 1% of the specific serum. Primary antibodies were: mouse anti-myosin 7a (1:1000, Developmental Studies Hybridoma Bank, NIH, Bethesda, MD, USA; #138-1C), rabbit anti-myosin 7a (1:200, Proteus Biosciences, Ramona, CA, USA; #25-6790), mouse anti-CtBP2 (C-terminal binding protein 2, 1:200, Biosciences, #612044) and mouse anti-GluR2 (AMPA-type glutamate receptor, 1:200, Millipore, Billerica, MA, USA; MAB397). All primary antibodies were labelled with species-appropriate Alexa Fluor secondary antibodies for 1 h at 37°C, and then washed three times (10 min) in PBS. Samples were then rinsed a final time in PBS (10 min) and mounted in Vectashield. The *z*-stack images were captured with a Nikon A1 confocal microscope (Nikon CFI Plan Apo 60× oil objective). The samples used to analyse the pillar–modiolar distribution of the synaptic ribbons were imaged using a Zeiss LSM 880 with AiryScan for super-resolution confocal microscopy. Both confocal microscopes are within the Wolfson Light Microscope Facility at the University of Sheffield. Image stacks were processed with Fiji ImageJ or Imaris analysis software.

The number and volume of synaptic ribbon puncta (and number of GluR2 puncta) was estimated from the *z*-stack images of the immunolabelled proteins using the Imaris software (Oxford Instruments, Abingdon, UK). Individual puncta were assigned to two separate groups (pillar or modiolar) using *k*-means clustering (a method of clustering each observation with the nearest mean, MacQueen, 1967) of their position along the pillar to modiolar axis with $k = 2$ clusters. Individual IHCs were manually identified and every protein punctum was automatically assigned to one IHC based on its centroid position.

Statistical analysis

Statistical comparisons of means were made by Student's two-tailed *t* test or, for multiple comparisons, analysis of variance (one-way or two-way ANOVA followed by a suitable *post hoc* test). $P < 0.05$ was selected as the criterion for statistical significance. Only mean values with a similar variance between groups were compared. Averages are quoted in the text and Figures as means ± SD. For tone burst ABR stimulus data, due to the presence of values outside the threshold limit of our equipment (95 dB), we used a non-parametric aligned ranks transformation two-way ANOVA, followed by Tukey's *post hoc* test or Mann–Whitney U-test with Bonferroni correction for pairwise comparisons. Data are quoted as median, and first and third quartiles.

Results

We performed experiments using four different mouse strains in order to provide a more comprehensive understanding of the pathophysiological differences between those with early-onset (C57BL/6J: **6J**, C57BL/6NTac: **6N**: Hequembourg & Liberman, 2001; Kane *et al.* 2012) and 'good hearing' late-onset hearing loss (C3H/HeJ: **C3H**: Trune *et al.* 1996). The early progression of hearing loss in 6J and 6N mice has been associated with a strain-specific hypomorphic allele in *Cadherin 23* (*Cdh23*^{ahl}: Johnson *et al.* 1997; Noben-Trauth *et al.* 2003). *Cdh23* encodes cadherin-23 that, together with protocadherin-15, forms the tip links required for gating the mechanoelectrical transducer channels (Kazmierczak *et al.* 2007; Richardson *et al.* 2011). When the mutation is corrected with CRISPR/Cas9 in 6N mice, C57BL/6NTac^{Cdh23+} mice (**6N-Repaired**) showed normal hearing at about 8 months of age (Mianné *et al.* 2016). Comparing 6N mice with the isogenic 6N-Repaired strain would allow us to identify the possible physiological influence of *Cdh23*^{ahl} in ageing. To identify possible common biological 'hallmarks' of

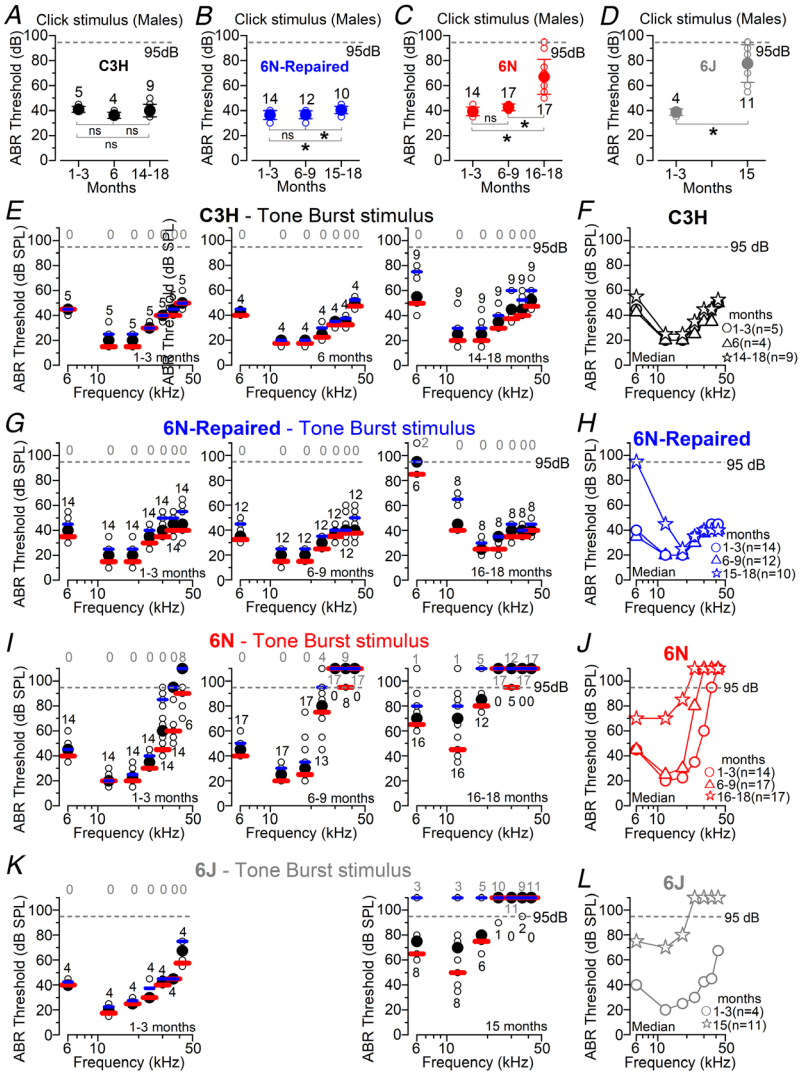

Figure 1. ABR thresholds evoked in ageing C3H, 6N, 6N-Repaired and 6J mice
A–D, average ABR thresholds for click stimuli recorded from male C3H (*A*), 6N-Repaired (*B*), 6N (*C*) and 6J (*D*) mice of increasing age. The number of mice tested for each age/strain is shown above or below the symbols. The dashed lines represent the upper threshold limit of our system (95 dB). Values are mean ± SD. The age range of the animal tested is shown on the *x*-axis. One-way ANOVA, Tukey's *post hoc* test: (*A*) 1–3 *vs.* 6–9 months $P = 0.2114$; 1–3 *vs.* 15–18 months $P = 0.8954$; 6–9 *vs.* 15–18 months $P = 0.2909$; (*B*) 1–3 *vs.* 6–9 months $P = 0.9804$; 1–3 *vs.* 15–18 months $P = 0.0113$; 6–9 *vs.* 15–18 months $P = 0.0222$; (*C*) 1–3 *vs.* 6–9 months $P = 0.5318$; for both 1–3 *vs.* 15–18 and 6–9 *vs.* 15–18 months $P < 0.0001$. Unpaired *t* test (*D*) $P = 0.0003$. *E–L*, ABR thresholds for frequency-specific pure tone stimulation from 6 to 42 kHz recorded from males C3H (*E*, *F*), 6N-Repaired (*G*, *H*), 6N (*I*, *J*) and 6J (*K*, *L*) mice at different ages. ABR data have been grouped into four different age ranges: 1–3, 6–9 and 15–18 months. Because of the several 'out of range' (i.e. above the upper threshold limit of our system, 95 dB) ABR threshold values at older ages in some strains, tone burst stimuli were plotted as median values (black symbols) and both the first (red lines) and third (blue lines) quartile ranges (*E*, *G*, *I*, *K*). Single data recordings are reported as open circles behind the median and quartiles. Right-hand panels (*F*, *H*, *J*, *L*) show the direct comparison of the median values only at different ages for the respective mouse strains. The number of mice tested for each age/strain is shown above or below the symbols. The grey numbers above the dashed line represent the number of mice with 'out-of-range' values. Statistical analysis for strain comparisons over the full range of frequencies tested at 14–18 months: $P = 0.9607$ for C3H *vs.* 6N-Repaired; $P < 0.0001$ for C3H *vs.* either 6N or 6J; $P < 0.0001$ for 6N-Repaired *vs.* either 6N or 6J; $P = 0.8700$ for 6N *vs.* 6J, Tukey's *post hoc* test, aligned ranks transformation two-way ANOVA. At the 12 kHz region and 14–18 months, statistical analysis for strain comparisons was significantly different between C3H and both 6N ($P = 0.0050$) and 6J ($P = 0.0157$); not significantly different for all other interactions: C3H *vs.* 6N-Repaired ($P = 0.1177$), 6N-Repaired *vs.* 6N ($P = 0.0914$) and 6J ($P = 0.0925$); 6N *vs.* 6J ($P = 0.6532$); aligned ranks transformation two-way ANOVA with Bonferroni adjustment.

cochlear ageing between genetically distinct good-hearing models, 6N-Repaired mice were compared to C3H mice.

Degree of hearing loss in different mouse strains

ABRs, which measure the summed activity of the auditory nerve fibres (e.g. Kujawa & Liberman, 2009), were used to investigate the hearing sensitivity of the above mouse strains kept under the same environmental conditions (Fig. 1). We found that for click ABR stimuli, C3H male mice showed no significant change in threshold with age ($P = 0.2075$, one way-ANOVA, Fig. 1*A*). Male 6N-Repaired, 6N and 6J mice showed significant increases in ABR thresholds with age (6N-Repaired, $P = 0.0082$, Fig. 1*B* and 6N: $P < 0.0001$, Fig. 1*C*, one way-ANOVA, for *post hoc* test see Fig. 1 legend; 6J: $P = 0.0003$, Fig. 1*D*, *t* test). Strain comparisons showed that ABR click thresholds over the entire age range investigated (Fig. 1*A–C*) were comparable between C3H and 6N-Repaired mice ($P = 0.8091$, Tukey's *post hoc* test, two-way ANOVA), but significantly elevated in the 6N strain (compared to both C3H and 6N-Repaired: $P < 0.0001$). ABR thresholds in 6J mice were also significantly elevated compared to both C3H and 6N-Repaired strains ($P < 0.0001$ for both comparisons), but not to 6N mice ($P = 0.3546$, Tukey's *post hoc* test, two-way ANOVA).

ABR thresholds for pure-tones (6, 12, 18, 24, 36, 42 kHz) were plotted for C3H (Figs 1*E, F* and 2*A*), 6N-Repaired (Figs 1*G, H* and 2*B*), 6N (Figs 1*I, J* and 2C) and 6J (Figs 1*K, L* and 2*D*) male mice. With age and over the 6–42 kHz range, ABR thresholds for pure-tones were significantly increased in 6N-Repaired, 6N and 6J ($P < 0.0001$, for all comparisons), but not in C3H mice ($P = 0.4215$, aligned ranks transformation two-way ANOVA). Strain comparison from aged mice (14–18 months) showed a highly significant difference in ABR thresholds for pure-tones (6–42 kHz range: $P < 0.0001$, aligned ranks transformation two-way ANOVA). 6N and 6J mice showed significantly elevated thresholds compared to both C3H and 6N-Repaired strains (*post hoc* test: see Fig. 1 legend). However, 6N-Repaired mice (Fig. 1*G* and *H*) showed comparable ABR thresholds to C3H mice for frequencies above 18 kHz (Fig. 1*E* and *F*), but were more similar to the isogenic 6N at lower frequencies (<18 kHz: Fig. 1*F* and *G*). At the 12 kHz region and 14–18 months, which was in the frequency range used to perform the single cell electrophysiological recordings (see below), 6N-Repaired mice exhibited an intermediate phenotype because the ABR threshold value was not significantly different from either the good hearing C3H mice nor from the early-onset hearing loss strains (6N and 6J) (statistical results: see Fig. 1 legend).

To provide some correlation between the ABR data and any possible morphological and/or physiological change identified in the *in vitro* work (see below), we analysed the amplitude and latency of the ABR wave I, which is generated by the summed response to sound of the afferent nerve fibres innervating the IHCs (Møller & Jannetta, 1982; Schaette & McAlpine, 2011). ABR wave I analysis was investigated at 12 kHz and at a value (75 dB) where signals could be recorded in all mice, even in those with high ABR thresholds (Fig. 3*A–E*). We found that wave I amplitude was significantly reduced in 6N, 6N-Repaired and 6J male mice between 1–3 months and either 6–9 or 15–18 months, but not in C3H mice (for statistical analysis see: Fig. 3*D*). Moreover, wave I latency increased with age only in 6N and 6J mice (Fig. 3*E*). We also found that in 6N mice, wave I amplitude was significantly reduced ($P = 0.0017$, Tukey's *post hoc* test, two-way ANOVA, overall

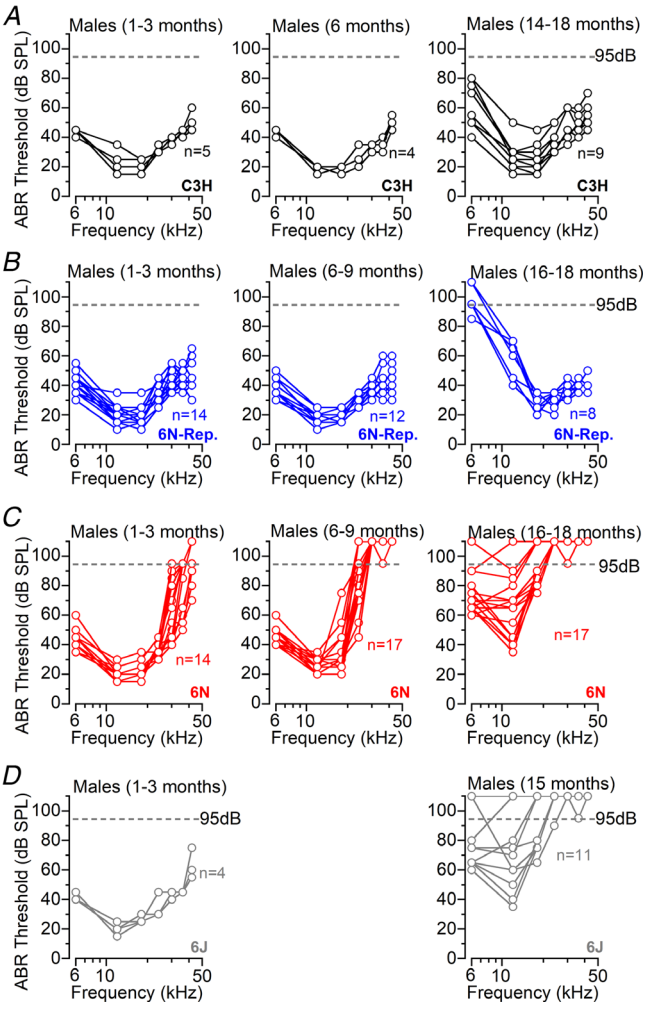

Figure 2. ABR thresholds evoked from individual ageing C3H, 6N, 6N-Repaired and 6J mice
A–D, ABR threshold recordings for frequency-specific pure tone stimulation from 6 to 42 kHz recorded from individual male C3H (*A*), 6N-Repaired (*B*), 6N (*C*) and 6J (*D*) mice using the same age ranges and data shown in Fig. 1. The dashed lines represent the upper intensity limit of our system, 95 dB. Data points above this line indicate recordings that did not show any auditory response at 95 dB.

strain effect) and latency increased ($P < 0.0001$) compared to 6N-Repaired mice. C3H mice had a similar wave I latency to 6N-Repaired ($P = 0.5557$), but a significantly reduced amplitude ($P = 0.0007$).

The above results have shown a well-defined hearing phenotype among the four mouse strains kept under the same environmental conditions. The level of hearing loss was found to be most severe for C57BL/6NTac and C57BL/6J, less so for C57BL/6NTac^{Cdh23+} and absent in C3H/HeJ, which like CBA mice show a very slow decline in their hearing thresholds with age (Spongr *et al.* 1997; Sha *et al.* 2008; Ohlemiller *et al.* 2010). Although the 6N-Repaired strain has an overall better hearing sensitivity than the isogenic 6N mice (Figs 1 and 2), the correction of the hypomorphic allele *Cdh23*^{ahl} (Mianné *et al.* 2016) had only a significant impact on frequencies at or above 12 kHz (Fig. 1). This indicates that progressive low-frequency hearing loss in C57BL/6NTac^{Cdh23+} (6N-Repaired) mice is not related to *Cdh23*^{ah}, but is instead probably due to a different strain-specific allele(s) present in C57BL/6NTac mice.

Exocytosis at IHC ribbon synapses is stable during ageing

We then investigated whether the different ABR thresholds and wave I among the different mouse strains were due to defects in exocytosis at IHC ribbon synapses with age. Sound-induced stimulation of the IHC stereociliary bundle generates a receptor potential that drives Ca^{2+}-dependent neurotransmitter release at their ribbon synapses. Synaptic vesicle exocytosis was measured as an increase in cell membrane capacitance (ΔC_m) that is interpreted as a sign of neurotransmitter release from presynaptic cells (e.g. Moser & Beutner, 2000; Johnson *et al.* 2005). Exocytosis at IHC ribbon synapses was investigated using whole-cell patch-clamp recordings from young adults (1 month) and aged (15–19 months) mice from the 9–12 kHz cochlear region.

We first investigated exocytosis from IHCs of male and female 6N mice. Figure 4*A* and *B* shows the maximal Ca^{2+} current (I_{Ca}) and the corresponding ΔC_m recorded from IHCs of 1- and 15–19-month-old 6N mice using a 50 ms

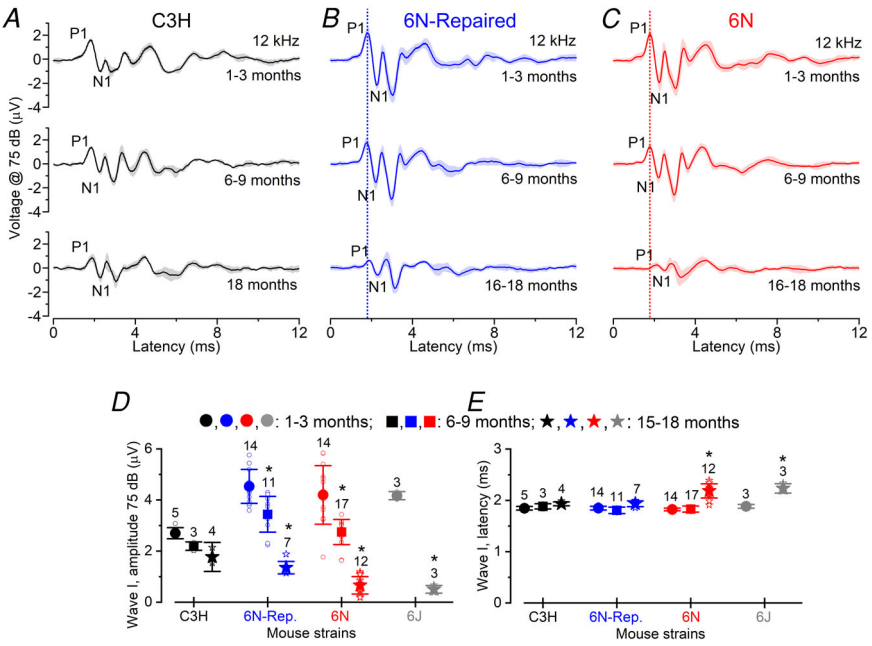

Figure 3. Changes in amplitude and latency of ABR wave in ageing mice
A–C, average ABR waveform responses at 12 kHz at 75 dB stimulus intensity in C3H (*A*), 6N-Repaired (*B*) and 6N (*C*) mice as a function of age. Continuous lines represent the average values and the shaded areas the SD. P1 and N1 indicate the positive and negative peaks of wave I. *D*, average amplitude of wave I (from P1 to N1) as a function of age in the four mouse strains. In 6N, 6N-Repaired and 6J mice, wave I amplitude was significantly reduced between 1–3 months and both 6–9 and 15–18 months ($P < 0.001$ for both comparisons: Tukey's *post hoc* test, one-way ANOVA or t-test). In C3H mice, wave I amplitude was $P > 0.05$ for all interactions. *E*, average latency of wave I (time between the onset of the stimulus and P1) as a function of age in the four mouse strains. In C3H and 6N-Repaired mice, there was no significant change in the wave I latency between 1–3 months and either 6–9 or 15–18 months ($P > 0.05$ for all interactions). For 6N, wave I latency did not significantly change between 1–3 and 6–9 months of age ($P > 0.05$), but increased between 6–9 and 15–18 months ($P < 0.001$) and 1–3 and 15–18 months ($P < 0.001$). In 6J, it also increased between 1–3 and 15–18 months ($P < 0.001$). The number of mice tested is shown above the data and single data points are plotted as small open symbols.

depolarizing voltage step (10 mV nominal increments) from −81 mV. The maximal size of I_{Ca} recorded in young-adult IHCs (−191 ± 82 pA, n = 6) was not significantly different to that recorded at 15–19 months (−154 ± 66 pA, n = 13, P = 0.2950, t test). The induced ΔC_m was also not significantly different with age (1 month: 20.0 ± 4.5 fF, n = 6; 15–19 months: 16.9 ± 8.0 fF, n = 13; P = 0.3940, t test). The rate of synaptic vesicle release in IHCs was studied by measuring ΔC_m in response to depolarizing voltage steps to −11 mV from −81 mV of varying duration from 2 ms to 1 s (interstep interval was at least 11 s), which allowed us to investigate the emptying of different synaptic vesicle pool populations (Fig. 4*C* and *D*). When performing experiments using physiological 1.3 mM extracellular Ca^{2+} and at body temperature, stimuli up to about 50 ms reveal the number of vesicles docked at the active zones (RRP) (Johnson *et al.* 2010, 2017). Longer steps induce the release of vesicles from a secondarily releasable pool (SRP) that is located further away from the Ca^{2+} channels (Moser & Beutner, 2000; Johnson *et al.* 2010, 2017). Voltage steps of up to about 50 ms (RRP) produced an increase in ΔC_m that could be approximated with a single exponential (Fig. 4*E*) under our experimental conditions. The initial release rate of the isolated RRP in 1-month-old IHCs (1067 ± 218 fF s^{-1} or 28,838 ± 5892 vesicles s^{-1}, n = 7) was not significantly different from those measured in 15-18 month old cells (894 ± 661 fF s^{-1} or 24,167 ± 17,852 vesicles s^{-1}, n = 11, P = 0.5166, t test). The size of the SRP was also not significantly different between IHCs recorded from young adults and aged mice (Fig. 4*D*, P = 0.9410, Bonferroni's *post hoc* test, two-way ANOVA).

A rate-limiting step in neurotransmitter release is the vesicle pool depletion/replenishment during prolonged repetitive stimulation. Therefore, we investigated whether vesicle release was limited by the relative pool refilling rates using a train of 50 ms steps to −11 mV (Fig. 4*F*). The RRP appears to be able to fully replenish following each step in both young adults and aged mice (Fig. 4*G* and *H*). The individual ΔC_m values were comparable in aged IHCs (9.44 ± 3.46 fF s^{-1}, mean ± SD, n = 8) and 1-month-old cells (11.27 ± 3.02 fF s^{-1}, n = 5, P = 0.3533, t test) (Fig. 4*H*).

Similar results to those observed in IHCs from the 6N strain were also recorded in 6N-Repaired (Fig. 5) and C3H (Fig. 6) male and female mice. These results indicate that the size, kinetics and replenishment of the synaptic vesicles in IHCs appear unaffected by any pathophysiological change occurring in the ageing cochlea.

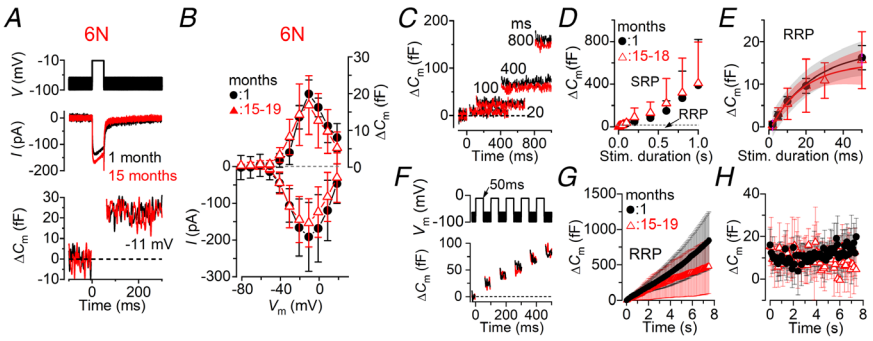

Figure 4. Size and kinetics of exocytosis in IHCs from ageing 6N mice
A, I_{Ca} and ΔC_m from IHCs of 1- and 15-month-old 6N mice. Recordings were obtained in response to 50 ms voltage steps from −81 mV in 10 mV increments. For clarity, only the peak responses at −11 mV are shown. *B*, average peak Ca^{2+} current–voltage (I–V_m, bottom panel) and capacitance–voltage (ΔC_m–V_m, top panel) curves from IHCs of 1 month (n = 6) and aged mice (15–19 months: n = 13). *C*, ΔC_m recordings from IHCs at 1 month (black) and 18 months (red) in response to voltage steps of different duration, which are used to recruit the readily releasable pool (RRP: <50 ms steps) and secondary releasable pool (SRP: >100 ms) of vesicles. *D*, average ΔC_m from 1-month-old (n = 6) and 15–18-month-old (n = 11) IHCs in response to voltage steps to −11 mV between 2 ms and 1 s (holding potential −81 mV) showing the RRP and SRP. *E*, size of the RRP (expanded from *D*) approximated with single exponential functions. Exponential fits from single IHC recordings were: 1 month ΔC_m = 15.7 ± 3.3 fF, τ = 15.0 ± 4.0 ms, n = 7; 15–18 months: ΔC_m = 16.2 ± 6.4 fF, τ = 22.1 ± 8.0 ms, n = 11 (P = 0.8488 and P = 0.0466, respectively, t test). The available RRP consisted of 423 ± 34 vesicles (1 month) and 437 ± 53 vesicles (15–18 months). *F*, ΔC_m elicited using repetitive voltage steps to −11 mV of 50 ms in duration in order to elicit the RRP (inter-step interval was 50 ms). For clarity, only the first few steps are shown. The voltage protocol used is shown above the traces. *G*, average cumulative ΔC_m values obtained in response to the 50 ms (75 steps) protocol, respectively, from 1-month-old (n = 5) and 15–18-month-old (n = 8) IHCs. *H*, individual ΔC_m values in 1- and 15–18-month-old IHCs measured following each voltage step from *G*. In this and Figures 5 and 6, data in *B*, *D*, *E*, *G* and *H* are reported as mean ± SD; *E* also shows the 95% confidence interval for the exponential fit curve.

Change in ribbon synapses number and volume in ageing IHCs

We then evaluated the number of afferent synapses in IHCs from all four mouse strains using antibodies to label the presynaptic ribbon protein RIBEYE (CtBP2) and the postsynaptic AMPA-type glutamate receptor GluR2 (e.g. Liberman *et al.* 2011; Furman *et al.* 2013). We found that both CtBP2 and GluR2 puncta were present at the IHC pre- and post-synaptic sites, respectively, in the 9–12 kHz cochlear region in all four aged mouse strains from both sexes (see Fig. 7*A* and *B* for 6N and 6N-Repaired mice). While the number of CtBP2 puncta in IHCs of C3H mice did not change significantly with age ($P > 0.05$ for all interactions, Tukey's *post hoc* test, one-way ANOVA, Fig. 7*C*), it was significantly reduced in the other three strains between 1 and 15 months (6N, 6N-Repaired, 6J: $P < 0.001$: Fig. 7*D*–*F*). No significant changes in CtBP2 puncta were detected between 1- and 6-month-old IHCs in both 6N and 6N-Repaired ($P > 0.05$). Strain comparison showed that the number of ribbons in IHCs from 6N-Repaired mice was significantly different compared to either C3H or 6N mice ($P < 0.0001$, two-way ANOVA), further supporting the *in vivo* finding (Figs 1–3) showing an 'intermediate severity' in the phenotype of this strain. We also found that the CtBP2 puncta were always closely colocalized with GluR2 labelling in IHCs from all four strains (Fig. 7*G* and *H*).

We then investigated possible changes in the distribution and volume of ribbon synapses in young adult and aged IHCs from mice of both sexes (Figs 8*A*–*K* and 9*A*–*H*). Afferent fibres have been shown to be spatially segregated around the IHC basolateral membrane of cats, such that low-spontaneous-rate fibres, which tend to have larger presynaptic ribbons, are more likely to contact their modiolar side, and high-spontaneous-rate fibres tend to contact the pillar side (Liberman, 1982*a*, 1990; Merchan-Perez & Liberman, 1996). The size of the ribbons was estimated by measuring their volume using the CtBP2 immunolabelling and super-resolution microscopy (Liberman *et al.* 2011; Furman *et al.* 2013). At 1 month, we found that IHCs from all mouse strains had a significantly larger ribbon volume on the modiolar compared to the pillar side (6N: $P = 0.0296$, 6J, 6N-Repaired and C3H: $P < 0.0001$, Sidak's *post hoc* test, one-way ANOVA, Figs 8*D*–*G* and 9*A*–*D*). With age, we observed an increased

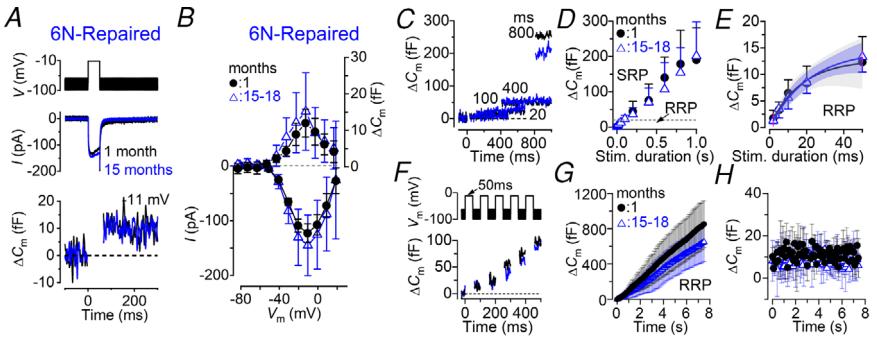

Figure 5. Size and kinetics of exocytosis in IHCs from ageing 6N-Repaired mice
A, I_{Ca} and ΔC_m from IHCs of 1- and 15-month-old mice. Recordings were obtained as described in Fig. 4. *B*, average peak Ca^{2+} current and ΔC_m curves from IHCs of 1-month-old ($n = 7$) and aged mice (15–18 months: $n = 11$). The maximal size of I_{Ca} recorded in young-adult IHCs (-123 ± 17 pA, $n = 7$) was not significantly different compared to that recorded at 15–18 months (-145 ± 55 pA, $n = 11$, $P = 0.3216$, *t* test). The induced ΔC_m was also not significantly reduced with age (1 month: 12.0 ± 3.8 fF, 15–18 months: 15.2 ± 8.3 fF, $P = 0.3555$, *t* test). *C*–*E*, rate of neurotransmitter release from six 1-month-old and six 15–18-month-old IHCs in response to voltage steps from 2 ms to 1 s (to -11 mV) showing the RRP and SRP (see main text). The size of the SRP was also not significantly different between IHCs recorded from young adults and aged mice ($P = 0.9563$, Bonferroni's *post hoc* test, two-way ANOVA). The size of the RRP in *E* (expanded from *D*) is approximated with single exponential functions. Exponential fits from single IHC recordings were: 1 month: $\Delta C_m = 12.1 \pm 5.3$ fF, $\tau = 13.6 \pm 6.5$ ms, $n = 6$; 15–18 months: $\Delta C_m = 14.4 \pm 3.1$ fF, $\tau = 20.9 \pm 7.0$ ms, $n = 6$ ($P = 0.3979$ and $P = 0.0910$, respectively, *t* test). The available RRP (mean ± SD) consisted of 328 ± 142 vesicles (1 month) and 388 ± 84 vesicles (15–18 months) ($P = 0.3979$). The initial release rate of the isolated RRP in 1-month-old IHCs (927 ± 182 fF s^{-1} or $25{,}057 \pm 4912$ vesicles s^{-1}, $n = 6$) was not significantly different from those measured in 15–18-month-old cells (741 ± 259 fF s^{-1} or $20{,}036 \pm 6997$ vesicles s^{-1}, $n = 6$, $P = 0.1807$, *t* test). *F*, ΔC_m elicited using repetitive voltage steps to -11 mV of 50 ms in duration in order to elicit the RRP (inter-step interval was 50 ms). *G*, average cumulative ΔC_m values obtained in response to the 50 ms (75 steps) protocol, respectively, from four 1-month-old and eight 15–18-month-old IHCs. *H*, individual ΔC_m values in 1-month-old and eight 15–18-month-old IHCs measured following each voltage step from *G*. The individual ΔC_m revealed that RRP refilling rate in aged IHCs was not significantly reduced (8.64 ± 2.56 fF s^{-1}, $n = 8$) compared to 1-month-old cells (11.36 ± 3.25 fF s^{-1}, $n = 4$, $P = 0.1419$, *t* test).

ribbon volume in both the modiolar and the pillar side in all strains, although it was much more pronounced in the 6J, 6N, 6N-Repaired (Figs 8*I–K* and 9*B–D*) than in C3H mice (Figs 8*H* and 9*A*). A previous serial-section ultrastructure study has shown that aged IHCs from 6J mice tend to exhibit synaptic active zones with multiple and larger ribbons compared to young adults (Stamataki *et al.* 2006). Although it is difficult to distinguish multiple ribbons from larger ribbons with immunostaining and fluorescence microscopy (Figs 7–9; see also Furman *et al.* 2013), we did not find any preferential localization of the larger puncta in either the modiolar or the pillar side of aged IHCs, in agreement with the electron microscopy study (Stamataki *et al.* 2006). We then investigated whether the reduction in ribbon number in ageing IHCs from all strains (Fig. 7*C–F*) had a preferential modiolar–pillar distribution. Using the same ribbon dataset used for volume estimation (Fig. 9*A–D*), which was a subset of those used in Fig. 7*C–F*, we found that ribbon number decreased with age on both the modiolar and the pillar sides of IHCs from both 6N ($P < 0.0001$, Sidak's *post hoc* test, two-way ANOVA) and 6J (modiolar $P < 0.0001$; pillar: $P = 0.0055$). In IHCs from the 6N-Repaired strain, ribbon number was significantly changed with age on the pillar ($P = 0.0074$) but not on the modiolar side ($P = 0.4446$). In C3H mice there was no significant change of ribbon number in both regions (modiolar: $P = 0.1798$; pillar: $P = 0.9366$) (Fig. 9 *E*).

Discussion

We have investigated age-related changes in the biophysical and morphological properties of IHC ribbon synapses in the 9–12 kHz cochlear region of four commonly used mouse strains with different progression of hearing loss (C57BL/6J, C57BL/6NTac, C57BL/6NTac^{Cdh23+} and C3H/HeJ). We found that with age, both modiolar and pillar sides of the IHC exhibited a loss of ribbon synapses but an increase in volume of the remaining ribbons. These changes correlate with the degree of hearing loss in the different mouse strains, being most severe for 6N and 6J, less so for 6N-Repaired and absent in C3H strains. Despite the changes in synapse morphology, we provided evidence that the size and kinetics of exocytosis, as well as the replenishment of synaptic vesicles, were not affected by age, indicating that a degree of compensation exists at ribbon synapses that could contribute to maintaining some degree of functionality in aged IHCs.

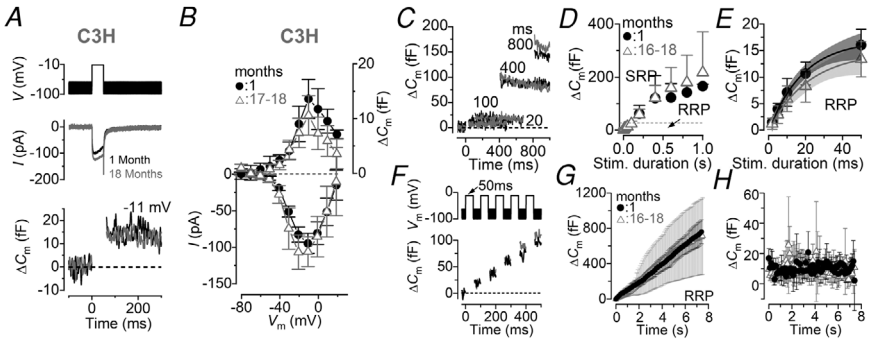

Figure 6. Size and kinetics of exocytosis in IHCs from ageing C3H mice
A, I_{Ca} and ΔC_m from IHCs of 1- and 18-month-old mice. Recordings were obtained as described in Fig. 4. *B*, average peak Ca^{2+} current and ΔC_m curves from IHCs of 1-month-old ($n = 5$) and aged mice (17–18 months: $n = 5$). The maximal size of I_{Ca} recorded in young-adult IHCs (-95 ± 14 pA, $n = 5$) was not significantly different compared to that recorded at 16–18 months (-106 ± 20 pA, $n = 5$, $P = 0.3282$, *t* test). The induced ΔC_m was also not significantly reduced with age (1 month: 13.6 ± 3.6 fF, 16–18 months: 10.6 ± 3.6 fF, $P = 0.2187$, *t* test). *C–E*, rate of neurotransmitter release from five 1-month-old and six 16–18-month-old IHCs in response to voltage steps from 2 ms to 1 s (to −11 mV) showing the RRP and SRP (see main text). The size of the SRP was also not significantly different between IHCs recorded from young adults and aged mice ($P = 0.8126$, Bonferroni's *post hoc* test, two-way ANOVA). The size of the RRP in *E* (expanded from *D*) is approximated with single exponential functions. Exponential fits from single IHC recordings were: 1 month: $\Delta C_m = 18.4 \pm 4.8$ fF, $\tau = 23.2 \pm 9.3$ ms, $n = 5$; 16–18 months: $\Delta C_m = 15.3 \pm 3.1$ fF, $\tau = 24.6 \pm 5.2$ ms, $n = 6$ ($P = 0.2150$ and $P = 0.7368$, respectively, *t* test). The available RRP consisted of 498 ± 129 vesicles, (1 month) and 412 ± 83 vesicles (16–18 months) ($P = 0.2150$). The initial release rate of the isolated RRP in 1-month-old IHCs (885 ± 354 fF s^{-1} or $23{,}925 \pm 9594$ vesicles s^{-1}, $n = 6$) was not significantly different from those measured in 15–18-month-old cells (660 ± 270 fF s^{-1} or $17{,}826 \pm 7298$ vesicles s^{-1}, $n = 6$, $P = 0.2609$, *t* test). *F*, ΔC_m elicited using repetitive voltage steps to −11 mV of 50 ms in duration in order to elicit the RRP (inter-step interval was 50 ms). *G*, average cumulative ΔC_m values obtained in response to the 50 ms (75 steps) protocol, respectively, from four 1-month-old and eight 16–18-month-old IHCs. *H*, individual ΔC_m values in 1-month-old and eight 16–18-month-old IHCs measured following each voltage step from *G*. The RRP refilling rate in aged IHCs was not significantly reduced (9.5 ± 4.3 fF s^{-1}, $n = 5$) compared to 1-month-old cells (10.2 ± 3.1 fF s^{-1}, $n = 5$, $P = 0.2995$).

Age-related morphological changes at IHC ribbon synapses

Type I fibres constitute the majority of SGNs that innervate the mammalian cochlea (~95%: Ryugo 1992). Each unbranched peripheral axon of these SGNs (Liberman, 1980) receives input from one IHC synapse, which normally contains only one ribbon, although some 20% of synapses appear to have multi-ribbon contacts (Merchan-Perez & Lieberman 1996; Michanski *et al.* 2019). Each IHC can drive the activity of up to ~20 SGNs depending on their frequency location along the mouse cochlea (Meyer *et al.* 2009). We found that in 15 month old IHCs, the number of ribbon synapses was lower in 6N and 6J strains, which suffered the worst hearing loss, than in 6N-repaired strain that had only partial hearing loss in the 9–12 kHz region. Although this is consistent with previous immunostaining observations in CBA/CaJ (Sergeyenko *et al.* 2013) and electron microscopy studies in 6J mice (Stamataki *et al.* 2006), we showed that it only becomes evident after 6 months of age. Interestingly, IHCs from C3H mice did not appear to lose synaptic ribbons with age but they had significantly fewer at young ages than IHCs from 6J, 6N and 6N-Repaired strains. The smaller number of synapses in C3H mice is likely to be compensated, at least in part, by having about 20% more IHCs in the 9–12 kHz region throughout life compared to the other three strains (unpublished data). Nevertheless,

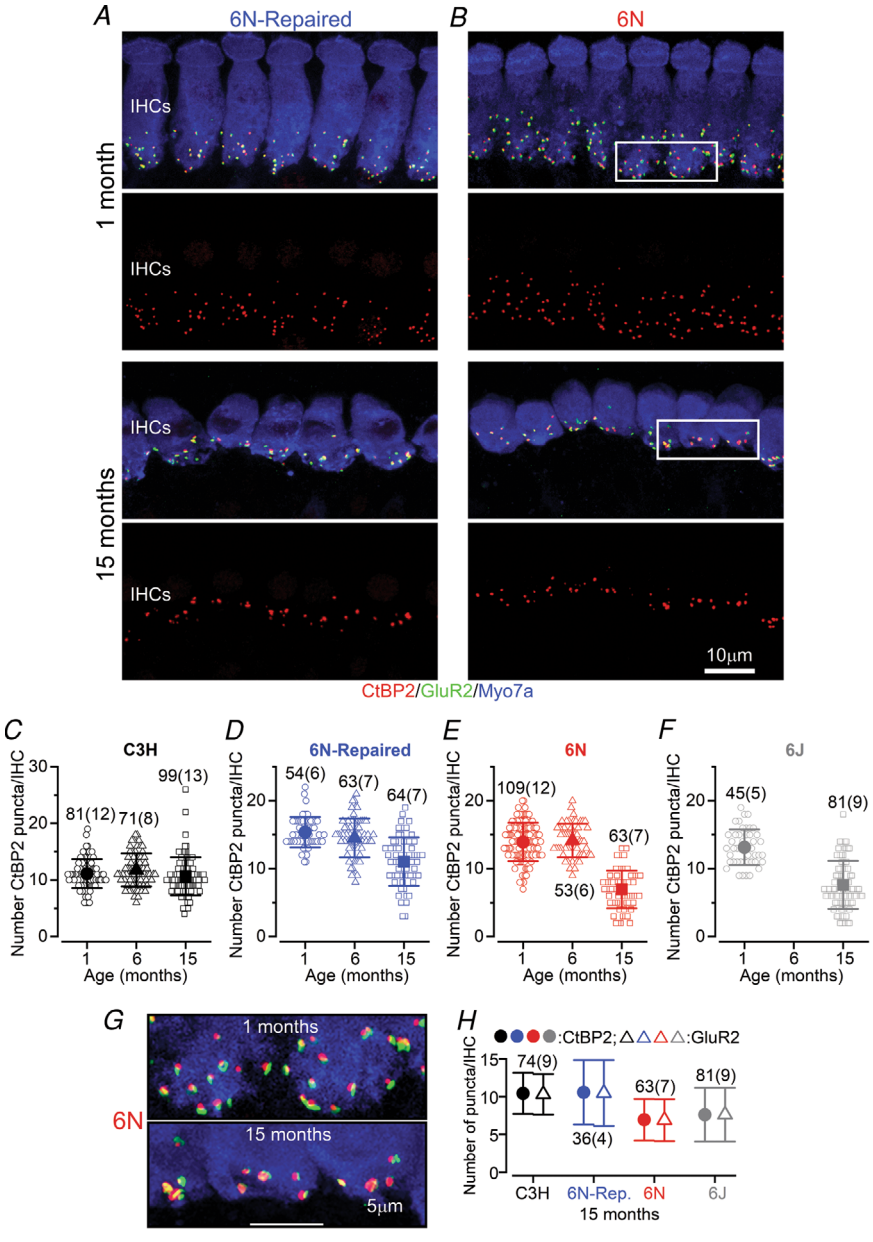

Figure 7. Ribbon synapse number is reduced in IHCs from most mouse strains
A and *B*, maximum intensity projections of confocal *z*-stacks of IHCs taken from the apical cochlear region (9–12 kHz) of 6N-Repaired (*A*) and 6N (*B*) mice at 1 and 15 months using antibodies against CtBP2 (ribbon synaptic marker: red) and GluR2 (postsynaptic marker: green). Myosin 7a (Myo7a) was used as the IHC marker (blue). Scale bar = 10 μm. *C–F*, number of CtBP2 puncta as a function of age in IHCs from C3H (*C*), 6N-Repaired (*D*), 6N (*E*) and 6J (*F*) mice. Data are plotted as mean values (larger closed symbols) and individual CtBP2 counts (smaller open symbols). *G*, enlarged view of the two regions highlighted (rectangular white boxes) in *B*, showing the juxtaposed CtBP2 (red) and GluR2 (green) puncta. *H*, number of CtBP2 and GluR2 puncta in IHCs from 15-month-old mice (C3H, 6N-Repaired, 6N and 6J). Numbers above or below the data in *C–F* and *H* represent the IHCs (and mice) used for each time point. Average values are mean ± SD.

a lower number of ribbons meant that C3H mice showed a significantly smaller wave I ABR amplitude at young ages compared to the other strains. Consistent with the correlation between synapse number and ABR response, the wave I amplitude was significantly reduced with age in 6N-Repaired and even more so in the 6J and 6N mice.

Cochlear ageing has been associated with loss of small afferent terminals in 6J mice (Stamataki *et al.* 2006), which in the cat have been described as the low spontaneous rate fibres (low-SR: Liberman, 1982*a*). This has also been seen in the ageing gerbil cochlea (Schmiedt *et al.* 1996). Since low-SR fibres seem to contact the modiolar side of IHCs in cats and guinea-pigs (Liberman, 1982*b*; Tsuji & Liberman, 1997), the expectation was that ageing would cause a significantly larger reduction in synaptic counts in this region. However, our data show a reduction in CtBP2 puncta in both the modiolar and pillar regions, with a more prominent decline in the pillar side. It is possible that the spatial distribution of low-SR (modiolar) and high-SR (pillar) afferent fibres around mouse IHCs is less segregated than in the cat. Some support for this hypothesis comes from a recent study showing that the intrinsic voltage-dependence characteristics of the presynaptic Ca^{2+} channels, which could be a key determinant of the different spontaneous and sound-evoked firing rate among SGNs, is highly variable in both modiolar and pillar sides of mouse cochlear IHCs (Ohn *et al.* 2016). Moreover, considerable variability in ribbon morphology was also reported within individual IHCs (Michanski *et al.* 2019). Finally, noise-induced neuropathy, which has been shown to selectively affect the low-SR fibres, caused an increase in the volume of the synaptic ribbons on both sides of the IHCs, although to a greater extent on the pillar side (Furman *et al.* 2013). Although the ribbon volume is normally greater on the modiolar side of young adult IHCs (Figs. 8, 9; for CBA/CaJ mice, see: Liberman *et al.* 2011), we found that with age the remaining ribbons on both IHC sides increased in volume. This finding further supports the idea that the loss of afferent fibres with age in mice is unlikely to be restricted to the modiolar side of IHCs. Alternatively, with age, ribbons may redistribute 'equally' around the

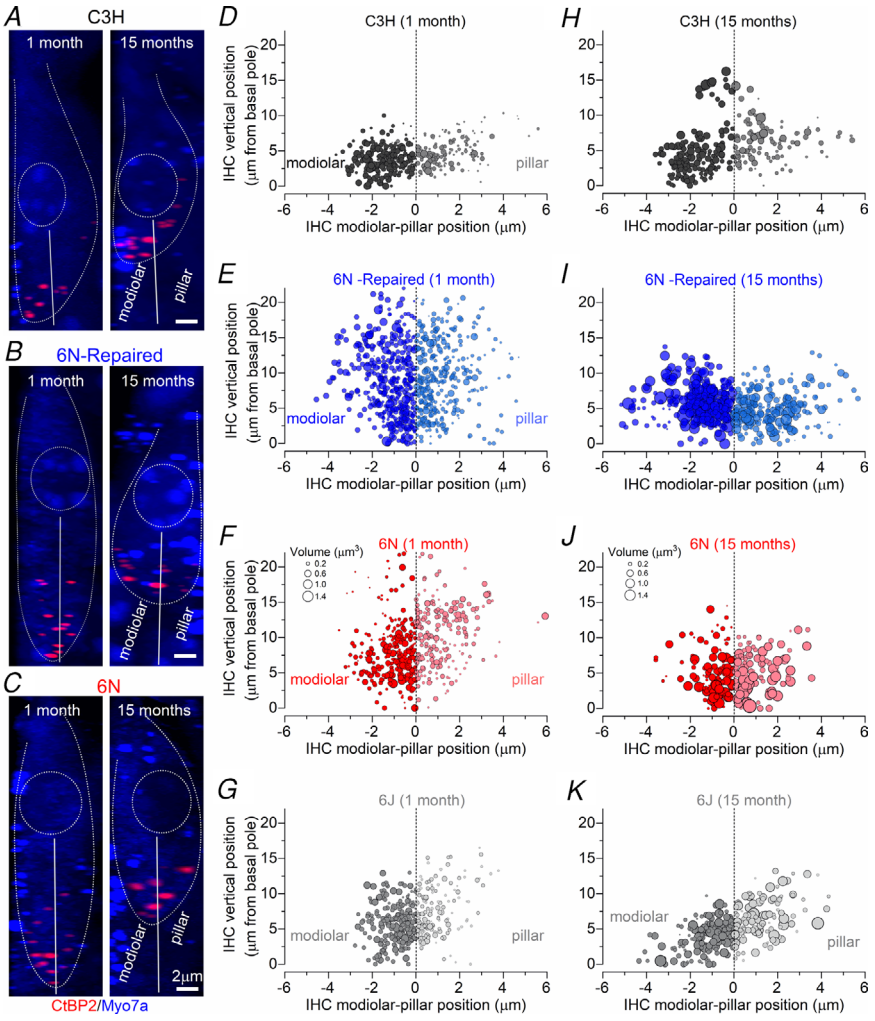

Figure 8. Changes in the volume and number of synaptic-ribbons with age
A–C, confocal *z*-stacks of IHCs taken from the apical cochlear region (9–12 kHz) of C3H (*A*), 6N-Repaired (*B*) and 6N (*C*) mice at 1 and 15 months using antibodies against CtBP2. Myosin 7a (Myo7a) was used as the IHC marker (blue). Dotted lines delineate the IHC surface and the nucleus. The continuous lines divide the modiolar and pillar side of the IHCs. Scale bar = 2 μm. *D–K*, bubble plots representing the distribution along the modiolar-to-pillar (horizontal) and cuticular-to-synaptic (vertical) direction of CtBP2 puncta (pooled data from several IHCs: see below). The marker size is proportional to the spot volume (scale volume in *F* and *J* also applies to all other panels). Data were collected from IHCs at 1 month (*D–G*) and 15 months (*H–K*) in C3H, 6N-Repaired, 6N and 6J mice. For number of IHCs and mice tested see Fig. 7.

IHC basal poles after the loss of low-SR fibres as previously suggested for noise-induced cochlear neuropathy (Furman *et al.* 2013). However, this seems unlikely since in IHCs of C3H mice the ribbons show some degree of volume increase on both the modiolar and pillar sides in aged IHCs, even though they show no synaptic loss.

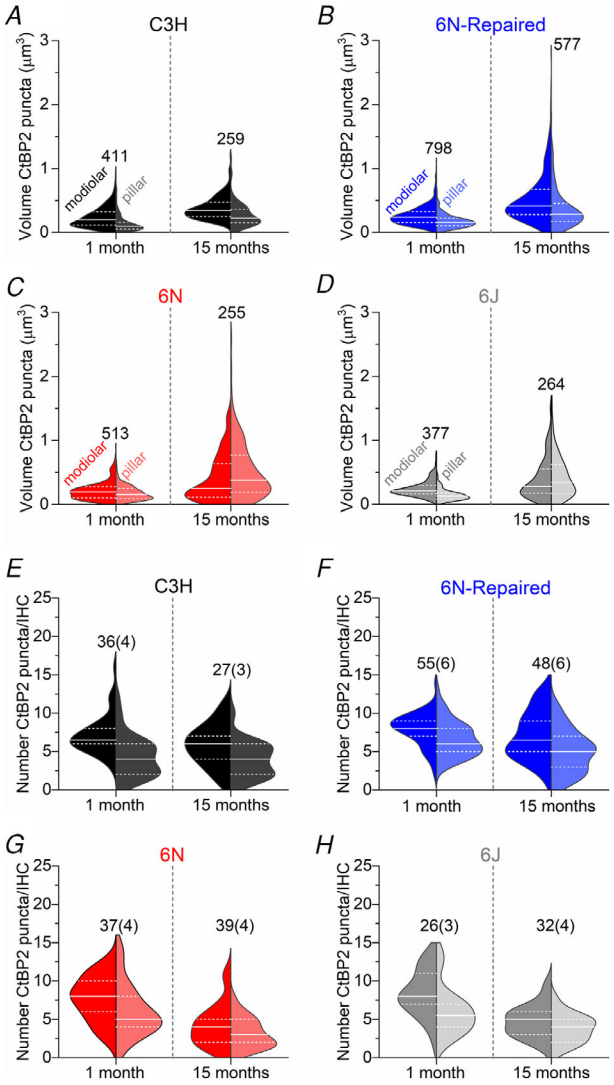

Figure 9. IHC modiolar–pillar gradient in the volume and number of synaptic-ribbons
A–D, violin plots comparing the modiolar–pillar distribution of ribbon volume in IHCs from 1 month (left plots) and 15 months (right plots) in C3H (*A*), 6N-Repaired (*B*), 6N (*C*) and 6J (*D*) mice (see Fig. 7). Both modiolar and pillar side show an increased CtBP2 volume in all mouse strains ($P < 0.0001$ for all interactions apart from that between 1 and 15 months; in the pillar side of C3H mice significance was $P = 0.0003$, Sidak's *post hoc* test, two-way ANOVA). *E–H*, violin plots comparing the modiolar–pillar distribution of ribbon number in IHCs from 1 month (left plots) and 15 months (right plots) in C3H (*E*), 6N-Repaired (*F*), 6N (*G*) and 6J (*H*) mice. The number of ribbons measured is shown above or next to the violin plots in *A–D*, while the number of IHCs (and mice) used is shown above the violin plots in *E–H*.

Functional changes at IHC ribbon synapses with age

Our estimates for the size and kinetics of neurotransmitter release and vesicle replenishment at ribbon synapses are remarkably similar between young (1 month) and old (15–19 months) IHCs from C3H and the other three strains showing a different progression of hearing loss. Considering the large age-related reduction in the number of ribbon synapses in 6J, 6N and 6N-Repaired, the apparently normal vesicle exocytosis indicates that ribbon synapses undergo major morphological re-organization. Compared to young adult IHCs, the bigger or multiple synaptic ribbons in aged IHCs have been shown to hold a significantly larger number of synaptic vesicles, both docked at the active zone and associated with the more distal pools (Stamataki *et al.* 2006). Afferent terminals onto IHCs are also significantly larger in aged mice, so despite the lower number of SGN endings, the overall synaptic area between IHCs and afferent terminals does not change significantly with age (Stamataki *et al.* 2006). The above morphological changes are also likely to be associated with a redistribution of the Ca^{2+} channels at the synaptic region (more channels per synapse). This is suggested by the similar kinetics of IHC exocytosis between mice that lose afferent synapses with age (6N and 6N-repaired mice) and those that did not (C3H mice). The significance of such morphological reorganization in aged IHCs is currently unclear but it closely resembles that seen during pre-hearing stages of development (Michanski *et al.* 2019), possibly as a mechanism that compensates for the loss of SNGs. A similar mechanism in which IHCs apparently recapitulate development has been seen in the aged cochlea, with the efferent system re-forming direct axo-somatic contacts with IHCs (Lauer *et al.* 2012; Zachary & Fuchs, 2015; unpublished data). This process seems to be linked with a malfunction of the mechano-electrical transducer (MET) channels (Corns *et al.* 2018).

Mechanisms leading to the progressive loss of ABR thresholds with age

We have demonstrated that the synaptic machinery of IHCs in mice undergoes several changes in the ageing cochlea (12 kHz cochlear region), with smaller numbers of larger synapses correlated with the level of hearing loss in mice. Despite these morphological changes, aged IHCs exhibited normal exocytotic responses, possibly leading to more glutamate-containing vesicles being released by the remaining larger SGN terminals. How these changes impact on the firing activity of the remaining SGNs is difficult to predict. Afferent firing activity depends on a combination of presynapstic (Merchan-Perez & Liberman, 1996; Grant *et al.* 2010; Ohn *et al.* 2016), postsynaptic (Liberman *et al.* 2011) and efferent (Yin *et al.* 2014) mechanisms, all of which change in the aged

cochlea (see above). The observed degree of functional compensation occurring at the IHC ribbon synapses, which could potentially act as a mechanism to preserve at least some hearing via the remaining SGN fibres, is unlikely to counteract the significant loss of SGN connections. Loss of IHC synapses and SGNs would have an impact on the normal encoding of the temporal properties of sound due to stochastic under-sampling (Lopez-Poveda, 2014), especially in noisy environments (Costalupes *et al.* 1984). As such, the proposed loss of low-SR fibres with age (Liberman, 1982*a*; Schmiedt *et al.* 1996; Stamataki *et al.* 2006), which also occurs during noise-exposure (Furman *et al.* 2013), cannot be the only cause of the wide range of ABR thresholds we observed among the different mouse strains. Other major contributing factors to the different hearing phenotypes among the mouse strains could arise from the differential loss of the electromotile outer hair cells (OHCs) (e.g. Francis *et al.* 2003; Sergeyenko *et al.* 2013), changes in IHC basolateral ion channel biophysics, efferent innervation and in the MET apparatus. Major changes in the number of hair cells in the 9–12 kHz cochlear region are unlikely, because we found comparable results among mouse strains exhibiting very different progressive hearing loss profiles (OHCs: Jeng *et al.* 2020*b*; IHCs: unpublished data). On the other hand, the degree of efferent fibres re-reforming axo–somatic connections with aged IHCs, which was demonstrated in C57BL/6J mice (Lauer *et al.* 2012; Zachary & Fuchs, 2015), was found to be correlated with the degree of hearing loss in the different mouse strains (Jeng *et al.* 2020*b*). The contribution of the MET current to the ageing hearing phenotype is supported by the observation that the structural and functional integrity of the stereociliary bundles is progressively altered with age (Bohne *et al.*, 1990; Bullen *et al.*, 2019) and that the hypomorphic *Cdh23*^{ahl} allele leads to early-onset hearing loss in several inbred mouse strains such as 6J (C57BL/6J) and 6N (C57BL/6NTac) mice (e.g. Johnson *et al.* 1997; Noben-Trauth *et al.* 2003). *Cdh23* encodes cadherin-23 that, together with protocadherin-15, forms the stereocilia tip links required for gating the mechano-electrical transducer channels (Kazmierczak *et al.* 2007). Mice harbouring the *Cdh23*^{ahl} allele show a reduced MET current in aged hair cells (OHCs: Jeng *et al.* 2020*b*; IHCs: unpublished data), but this was not observed in 6N-Repaired mice (unpublished data).

We also found that mice in which the *Cdh23*^{ahl} allele was repaired with targeted CRISPR/Cas9 gene editing (6N-Repaired: Mianné *et al.* 2016) exhibited age-related high-frequency hearing thresholds comparable to mouse strains that innately carry the wild-type *Cdh23* allele (e.g. C3H). However, both the 6N and the 6N-Repaired mice exhibit a comparable progressive low-frequency hearing loss (<18 kHz), which, therefore, is not related to *Cdh23*, but is likely to be due to a different strain-specific allele(s) in C57BL/6NTac mice.

References

Bohne BA, Gruner MM & Harding GW (1990). Morphological correlates of aging in the chinchilla cochlea. *Hear Res* **48**, 79–91.

Bowl MR & Dawson SJ (2019). Age-related hearing loss. *Cold Spring Harb Perspect Med* **9**, a033217.

Brandt A, Striessnig J & Moser T (2003). $Ca_V1.3$ channels are essential for development and presynaptic activity of cochlear inner hair cells. *J Neurosci* **23**, 10832–10840.

Bullen A, Forge A, Wright A, Richardson GP, Goodyear RJ & Taylor R (2019). Ultrastructural defects in stereocilia and tectorial membrane in aging mouse and human cochleae. *J Neurosci Res.* https://doi.org/10.1002/jnr.24556.

Ceriani F, Hendry A, Jeng JY, Johnson SL, Stephani F, Olt J, Holley MC, Mammano F, Engel J, Kros CJ, Simmons DD & Marcotti W (2019). Coordinated calcium signalling in cochlear sensory and non-sensory cells refines afferent innervation of outer hair cells. *EMBO J* **38**, e99839.

Corns LF, Johnson SL, Roberts T, Ranatunga KM, Hendry A, Ceriani F, Safieddine S, Steel KP, Forge A, Petit C, Furness DN, Kros CJ & Marcotti W (2018). Mechanotransduction is required for establishing and maintaining mature inner hair cells and regulating efferent innervation. *Nature Comm* **9**, 4015.

Costalupes JA, Young ED & Gibson DJ (1984). Effects of continuous noise backgrounds on rate response of auditory nerve fibers in cat. *J Neurophysiol* **51**, 1326–1344.

Francis HW, Ryugo DK, Gorelikow MJ, Prosen CA & May BJ (2003). The functional age of hearing loss in a mouse model of presbycusis. II. Neuroanatomical correlates. *Hear Res* **183**, 29–36.

Frank T, Rutherford MA, Strenzke N, Neef A, Pangršič T, Khimich D, Fejtova A, Gundelfinger ED, Liberman MC, Harke B, Bryan KE, Lee A, Egner A, Riedel D & Moser T (2010). Bassoon and the synaptic ribbon organize Ca^{2+} channels and vesicles to add release sites and promote refilling. *Neuron* **68**, 724–738.

Furman AC, Kujawa SG & Liberman MC (2013). Noise-induced cochlear neuropathy is selective for fibers with low spontaneous rates. *J Neurophysiol* **110**, 577–586.

Gates GA & Mills JH (2005). Presbycusis. *Lancet* **366**, 1111–1120.

Glowatzki E & Fuchs PA (2002). Transmitter release at the hair cell ribbon synapse. *Nat Neurosci* **5**, 147–154.

Goutman JD & Glowatzki E (2007). Time course and calcium dependence of transmitter release at a single ribbon synapse. *Proc Natl Acad Sci U S A* **104**, 16341–16346.

Gordon-Salant S (2005). Hearing loss and aging: new research findings and clinical implications. *J Rehabil Res Dev* **42**, 9–24.

Grant L, Yi E & Glowatzki E (2010). Two modes of release shape the postsynaptic response at the inner hair cell ribbon synapse. *J Neurosci* **30**, 4210–4220.

Hequembourg S & Liberman MC (2001). Spiral ligament pathology: a major aspect of age-related cochlear degeneration in C57BL/6 mice. *J Assoc Res Otolaryngol* **2**, 118–129.

Kane KL, Longo-Guess CM, Gagnon LH, Ding D, Salvi RJ & Johnson KR (2012). Genetic background effects on age-related hearing loss associated with Cdh23 variants in mice. *Hear Res* **283**, 80–88.

Kazmierczak P, Sakaguchi H, Tokita J, Wilson-Kubalek EM, Milligan RA, Müller U & Kachar B (2007) Cadherin 23 and protocadherin 15 interact to form tip-link filaments in sensory hair cells. *Nature* **449**, 87–91.

Keen EC & Hudspeth AJ (2006). Transfer characteristics of the hair cell's afferent synapse. *Proc Natl Acad Sci U S A* **103**, 5537–5542.

Kujawa SG & Liberman MC (2009). Adding insult to injury: cochlear nerve degeneration after "temporary" noise-induced hearing loss. *J Neurosci* **29**, 14077–14085.

Kujawa SG & Liberman MC (2015). Synaptopathy in the noise-exposed and aging cochlea: primary neural degeneration in acquired sensorineural hearing loss. *Hear Res* **330**, 191–199.

Ingham NJ, Pearson S & Steel KP (2011). Using the auditory brainstem response (ABR) to determine sensitivity of hearing in mutant mice. *Curr Protoc Mouse Biol* **1**, 279–287.

Jeng JY, Ceriani F, Hendry A, Johnson SL, Yen P, Simmons DD, Kros CJ & Marcotti W (2020*a*) Hair cell maturation is differentially regulated along the tonotopic axis of the mammalian cochlea. *J Physiol* **598**, 151–170.

Jeng J-Y, Johnson SL, Carlton AJ, De Tomasi L, Goodyear R, De Faveri F, Furness DN, Wells S, Brown SDM, Holley MC, Richardson GP, Mustapha M, Bowl MR & Marcotti W (2020*b*) Age-related changes in the biophysical and morphological characteristics of mouse cochlear outer hair cells. *J Physiol* **598**, 3891–3910.

Johnsson LG (1974). Sequence of degeneration of Corti's organ and its first-order neurons. *Ann Otol Rhinol Laryngol* **83**, 294–303.

Johnson KR, Erway LC, Cook SA, Willott JF & Zheng QY (1997). A major gene affecting age-related hearing loss in C57BL/6J mice. *Hear Res* **114**, 83–92.

Johnson SL, Marcotti W & Kros CJ (2005). Increase in efficiency and reduction in Ca^{2+} dependence of exocytosis during development of mouse inner hair cells. *J Physiol* **563**, 177–191.

Johnson SL, Forge A, Knipper M, Münkner S & Marcotti W (2008). Tonotopic variation in the calcium dependence of neurotransmitter release and vesicle pool replenishment at mammalian auditory ribbon synapses. *J Neurosci* **28**, 7670–7678.

Johnson SL, Franz C, Kuhn S, Furness DN, Rüttiger L, Münkner S, Rivolta MN, Seward EP, Herschman HR, Engel J, Knipper M & Marcotti W (2010). Synaptotagmin IV determines the linear Ca^{2+} dependence of vesicle fusion at auditory ribbon synapses. *Nat Neurosci* **13**, 45–52.

Johnson SL, Kuhn S, Franz C, Ingham N, Furness DN, Knipper M, Steel KP, Adelman JP, Holley MC & Marcotti W (2013). Presynaptic maturation in auditory hair cells requires a critical period of sensory-independent spiking activity. *Proc Natl Acad Sci U S A* **110**, 8720-8725.

Johnson SL, Olt J, Cho S, von Gersdorff H & Marcotti W (2017). The coupling between Ca^{2+} channels and the exocytotic Ca^{2+} sensor at hair cell ribbon synapses varies tonotopically along the mature cochlea. *J Neurosci* **37**, 2471–2484.

Johnson SL, Safieddine S, Mustapha M & Marcotti W (2019). Hair cell afferent synapses: function and dysfunction. *Cold Spring Harb Perspect Med* **9**, pii: a033175.

Lauer AM, Fuchs PA, Ryugo DK & Francis HW (2012). Efferent synapses return to inner hair cells in the aging cochlea. *Neurobiol Aging* **33**, 2892–2902.

Lenzi D, Runyeon JW, Crum J, Ellisman MH & Roberts WM (1999). Synaptic vesicle populations in saccular hair cells reconstructed by electron tomography. *J Neurosci* **19**, 119–132.

Liberman MC (1978). Auditory-nerve response from cats raised in a low-noise chamber. *J Acoust Soc Am* **63**, 442–455

Liberman MC (1980). Morphological differences among radial afferent fibers in the cat cochlea: an electron-microscopic study of serial sections. *Hear Res* **3**, 45–63.

Liberman MC (1982*a*). The cochlear frequency map for the cat: Labeling auditory-nerve fibers of known characteristic frequency. *J Acoust Soc Am* **72**, 1441–1449.

Liberman MC (1982*b*). Single-neuron labeling in the cat auditory nerve. *Science* **216**, 1239–1241.

Liberman MC, Dodds LW & Pierce S (1990). Afferent and efferent innervation of the cat cochlea: quantitative analysis with light and electron microscopy. *J Comp Neurol* **301**, 443–460

Liberman LD, Wang H & Liberman MC (2011). Opposing gradients of ribbon size and AMPA receptor expression underlie sensitivity differences among cochlear-nerve/hair-cell synapses. *J Neurosci* **31**, 801–808.

Lopez-Poveda EA (2014). Why do I hear but not understand? Stochastic undersampling as a model of degraded neural encoding of speech. *Front Neurosci* **8**, 348.

Marcotti W, Johnson SL, Holley MC & Kros CJ (2003). Developmental changes in the expression of potassium currents of embryonic, neonatal and mature mouse inner hair cells. *J Physiol* **548**, 383–400

Marcotti W, Johnson SL & Kros CJ (2004). Effects of intracellular stores and extracellular Ca^{2+} on Ca^{2+}-activated K^+ currents in mature mouse inner hair cells. *J Physiol* **557**, 613-33

MacQueen JB (1967). Some methods for classification and analysis of multivariate observations. *Math Statist Prob* **1**: 281–297.

Merchan-Perez A & Liberman MC (1996). Ultrastructural differences among afferent synapses on cochlear hair cells: correlations with spontaneous discharge rate. *J Comp Neurol* **371**, 208–221.

Meyer AC, Frank T, Khimich D, Hoch G, Riedel D, Chapochnikov NM, Yarin YM, Harke B, Hell SW, Egner A & Moser T (2009). Tuning of synapse number, structure and function in the cochlea. *Nat Neurosci* **12**, 444–453.

Mianné J, Chessum L, Kumar S, Aguilar C, Codner G, Hutchison M, Parker A, Mallon AM, Wells S, Simon MM, Teboul L, Brown SD & Bowl MR (2016). Correction of the auditory phenotype in C57BL/6N mice via CRISPR/Cas9-mediated homology directed repair. *Genome Med* **8**, 16.

Michanski S, Smaluch K, Steyer AM, Chakrabarti R, Setz C, Oestreicher D, Fischer C, Möbius W, Moser T, Vogl C & Wichmann C (2019). Mapping developmental maturation of inner hair cell ribbon synapses in the apical mouse cochlea. *Proc Natl Acad Sci U S A* **116**, 6415-6424.

Møller A & Jannetta P (1982). Evoked potentials from the inferior colliculus in man. *Electroencephalogr Clin Neurophysiol* **53**, 612–620.

Moser T & Beutner D (2000). Kinetics of exocytosis and endocytosis at the cochlear inner hair cell afferent synapse of the mouse. *Proc Natl Acad Sci U S A* **97**, 883–888.

Müller M, von Hünerbein K, Hoidis S & Smolders JW (2005). A physiological place-frequency map of the cochlea in the CBA/J mouse. *Hear Res* **202**, 63–73.

Noben-Trauth K, Zheng QY & Johnson KR (2003). Association of cadherin 23 with polygenic inheritance andgenetic modification of sensorineural hearing loss. *Nat Genet* **35**, 21–23.

Ohlemiller KK, Dahl AR & Gagnon PM (2010). Divergent aging characteristics in CBA/J and CBA/CaJ mouse cochleae. *J Assoc Res Otolaryngol* **11**, 605–623.

Ohlemiller KK, Jones SM & Johnson KR (2016). Application of mouse models to research in hearing and balance. *J Assoc Res Otolaryngol* **17**, 493–523.

Ohn TL, Rutherford MA, Jing Z, Jung S, Duque-Afonso CJ, Hoch G, Picher MM, Scharinger A, Strenzke N & Moser T (2016) Hair cells use active zones with different voltage dependence of Ca^{2+} influx to decompose sounds into complementary neural codes. *Proc Natl Acad Sci U S A* **113**, E4716-25.

Platzer J, Engel J, Schrott-Fischer A, Stephan K, Bova S, Chen H, Zheng H & Striessnig J (2000). Congenital deafness and sinoatrial node dysfunction in mice lacking class D L-type Ca^{2+} channels. *Cell* **102**, 89–97.

Richardson GP, de Monvel JB & Petit C (2011). How the genetics of deafness illuminates auditory physiology. *Annu Rev Physiol* **73**, 311–334.

Pujol R, Lavigne-Rebillard M & Lenoir M (1998). Development of sensory and neural structures in the mammalian cochlea. In *Development of the Auditory System*, eds. Rubel EW, Popper AN & Fay RR, pp. 146–192. Springer, New York.

Ryugo DK. 1992. The auditory nerve: Peripheral innervation, cell body morphology, and central projections. In *The Mammalian Auditory Pathway: Neuroanatomy*, eds. Webster DB, Fay RR, pp. 23–65. Springer, New York.

Schaette R & McAlpine D (2011). Tinnitus with a normal audiogram: physiological evidence for hidden hearing loss and computational model. *J Neurosci* **31**, 13452-13457.

Schmiedt RA, Mills JH & Boettcher FA (1996). Age-related loss of activity of auditory-nerve fibers. *J Neurophysiol* **76**, 2799–2803.

Schuknecht HF & Gacek MR (1993). Cochlear pathology in presbycusis. *Ann Otol Rhinol Laryngol* **102**, 1–16.

Sergeyenko Y, Lall K, Liberman MC & Kujawa SG (2013). Age-related cochlear synaptopathy: an early-onset contributor to auditory functional decline. *J Neurosci* **33**, 13686–13694.

Sha SH, Kanicki A, Dootz G, Talaska AE, Halsey K, Dolan D, Altschuler R & Schacht J (2008). Age-related auditory pathology in the CBA/J mouse. *Hear Res* **243**, 87–94.

Spongr VP, Flood DG, Frisina RD & Salvi RJ (1997). Quantitative measures of hair cell loss in CBA and C57BL/6 mice throughout their life spans. *J Acoust Soc Am* **101**, 3546–3553.

Stamataki S, Francis HW, Lehar M, May BJ & Ryugo DK (2006). Synaptic alterations at inner hair cells precede spiral ganglion cell loss in aging C57BL/6J mice. *Hear Res* **221**, 104–118.

Trune DR, Kempton JB & Mitchell C (1996). Auditory function in the C3H/HeJ and C3H/HeSnJ mouse strains. *Hear Res* **96**, 41–45.

Tsuji J & Liberman MC (1997). Intracellular labeling of auditory nerve fibers in guinea pig: central and peripheral projections. *J Comp Neurol* **381**, 188–202.

Virtanen P, Gommers R, Oliphant TE, Haberland M, Reddy T, Cournapeau D, Burovski E, Peterson P, Weckesser W, Bright J, van derWalt SJ, Brett M, Wilson J, Millman KJ, Mayorov N, Nelson ARJ, Jones E, Kern R, Larson E, Carey CJ, Polat İ, Feng Y, Moore EW, Van der Plas J, Laxalde D, Perktold J, Cimrman R, Henriksen I, Quintero EA, Harris CR, Archibald AM, Ribeiro AH, Pedregosa F & vanMulbregt P (2020). SciPy 1.0–fundamental algorithms for scientific computing in python. *Nat Methods* **17**, 261–272.

Winter IM, Robertson D & Yates GK (1990). Diversity of characteristic frequency rate-intensity functions in guinea pig auditory nerve fibres. *Hear Res* **45**, 191–202

Wong AB, Rutherford MA, Gabrielaitis M, Pangrsic T, Göttfert F, Frank T, Michanski S, Hell S, Wolf F, Wichmann C & Moser T (2014). Developmental refinement of hair cell synapses tightens the coupling of Ca^{2+} influx to exocytosis. *EMBO J* **33**, 247–264.

Wu PZ, Liberman LD, Bennett K, de Gruttola V, O'Malley JT, Liberman MC (2019). Primary neural degeneration in the human cochlea: evidence for hidden hearing loss in the aging ear. *Neurosci* **407**, 8–20.

Yin Y, Liberman LD, Maison SF & Liberman MC (2014). Olivocochlear innervation maintains the normal modiolar-pillar and habenular-cuticular gradients in cochlear synaptic morphology. *J Assoc Res Otolaryngol* **15**, 571–583.

Zachary SP & Fuchs PA (2015). Re-emergent inhibition of cochlear inner hair cells in a mouse model of hearing loss. *J Neurosci* **35**, 9701–9706.

Zampini V, Johnson SL, Franz C, Knipper M, Holley MC, Magistretti J, Masetto S & Marcotti W (2013). Burst activity and ultrafast activation kinetics of CaV1.3 Ca^{2+} channels support presynaptic activity in adult gerbil hair cell ribbon synapses. *J Physiol* **591**, 3811–3820.

Additional information

Competing interests

The authors declare no conflicts of interest.

Authors contributions

J-Y.J., F.C., J.O., S.L.J. and W.M. were involved in the acquisition, analysis or interpretation of the data. S.D.B., M.C.H. and M.R.B.

were involved in the initial design and interpretation of data. All authors were involved in revising it critically for important intellectual content. J-Y.J. and W.M. conceived and designed the study and drafted the paper. All authors approved the final version of the manuscript. All authors agree to be accountable for all aspects of the work in ensuring that questions related to the accuracy or integrity of any part of the work are appropriately investigated and resolved. All persons designated as authors qualify for authorship, and all those who qualify for authorship are listed

Funding

This work was supported by the: Wellcome Trust (102892/Z/13/Z) to W.M.; Medical Research Council (MC/UP/1503/2) to M.R.B and (MR/S002510/1) to M.M.

Acknowledgements

The authors thank Lukas Rüttiger and Neil Ingham for advice on the ABR experiments and analysis, and Michelle Bird (University of Sheffield) for her assistance with the mouse husbandry. The data that support the findings of this study are available from the corresponding author upon reasonable request.

Keywords

age-related hearing loss, auditory brainstem responses, calcium channels, cochlea, exocytosis, inner hair cells, mouse, ribbon synapses

Supporting information

Additional supporting information may be found online in the Supporting Information section at the end of the article.

Statistical Summary Document